14

Single and Double Laser Pulse Interaction with Solid State – Application to Plasma Spectroscopy

Richard Viskup
Johannes Kepler University Linz, Institute of Applied Physics, Linz
Austria

1. Introduction

When a nanosecond laser pulse with sufficiently high laser energy is focused into a solid-state surface, pulsed laser ablation of the material and subsequently laser induced plasma formation occurs. An emitting light from a plasma is a rich source of information and its optical emission is something like "fingerprints" of emitting atomic, ionic and molecular species, composed in the irradiated sample. This emission can be used for the basic spectrochemical analysis of the studied material's composition. Laser induced plasma spectroscopy is an emerging technique for fast and accurate compositional analysis of many different materials (Viskup, 2010), and is nowadays, very often used in diverse applications. However, the issue of sensitivity and detection limits are still open question. A main goal of this chapter is to shown the possibility to enhance an optical emission from plasma and improve a limit of detection of trace elements detected by optical emission from a measured sample. For this purpose, the advantage of double laser pulse irradiation is very convenient for plasma re-heating or re-excitation (Viskup et al., 2010).

The double-pulse irradiation was proposed for more efficient production of analyte species in excited states. It uses two laser pulses for excitation with a defined delay time between pulses typically in the order of ns or μs. One of the first articles about the double-pulse configuration was published by (Cremers et al., 1984). Collinear double pulse studies of solid state in a gas atmosphere were first reported in the mid nineties, in (Sattmann et al., 1995). The technique has been re-investigated especially in the last decade for a broad range of materials and for many different measurement parameters, including the use of ultrashort femtosecond or picosecond laser pulses in (Noll et al., 2004; Semerok et al., 2004; Babushok et al., 2006). The technique splits into two main streams: First the collinear double-pulse geometry (Gautier et al., 2005: Peter et al., 2007), where two laser beams are delivered on the same target surface along the same optical path, and the second the orthogonal geometry (Cristoforetti et al., 2006; Choi et al., 2009), where only one pulse ablates the sample surface. The double-pulse irradiation approach has received some attention in the scientific community due to the considerable signal enhancement observed for some materials.

This chapter is dedicated to single and double laser pulse interaction with main emphases into application to spectroscopy. Research has been dedicated to systematic studies of

collinear nanosecond double-pulse measurements, and to double pulse plasma plume characterization. A comparison between single pulse and a double pulse laser irradiation by means of time resolved plasma plume photography and plasma spectroscopy are presented. The optimal parameters for double pulse exposure, especially for pulse to pulse separation time is considered. Results of this research should contribute to a better understanding of single and double nanosecond laser pulse interaction with solid-state material. By setting up of optimal parameters for double pulse laser interaction, it is possible to improve plasma emission from studied sample for industrial or scientific applications.

2. Characterization of nanosecond laser induced plasma

2.1 Plasma formation

When a nanosecond laser pulse is focused into solid-state surface with sufficient energy of the radiation to induce material vaporization, a dense vapour plume can be formed. This vapour consists of clusters, molecules, atoms, ions, electrons and scatter radiation. Species, which are ejecting from the surface, take along some kinetic and internal energy. Clusters are formed due to collective effects and droplets formation are related to hydrodynamic perturbations, big material fragments are ejected due to stress relaxation. This phenomenon can affect also the average energy per atom required for material removal, which can be then significantly smaller. Thermalization of species which are leaving from the surface is performed via collisions within few mean free paths from the sample surface, which is known as Knudsen layer. The plume generated at the surface has a strongly forwarded direction due to high temperature and pressure gradients in the axial direction, compared to gradients in the lateral directions. The simplest model (Anisimov et al., 1993) considers the expansion of the vapour beyond the Knudsen layer, and is described by an adiabatically expanding gas. Model predicts the temperature gradients within the plume with increasing distance from the source. In general the species leaving from the substrate surface generate recoil pressure on the substrate. In the presence of a molten surface layer, generated by the focused laser beam irradiation the recoil pressure expels the liquid from the surface. This is schematically shown in Figure 1. The ablated material may also generate a shock wave and the vapour plume absorbs the scatter incident laser radiation.

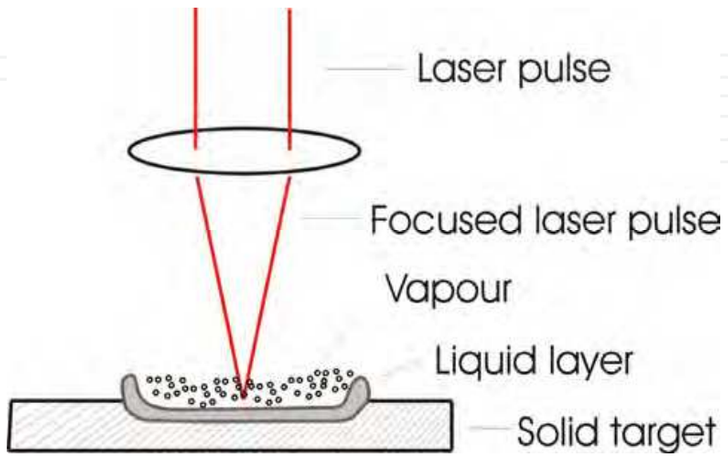

Fig. 1. Schematic interpretation of laser induced surface melting, vaporization and liquid phase expulsion.

With increasing laser light intensity an increasing fraction of atoms and molecules become ionized. After the substantial ionization, it can be described as plasma. With formation of the plasma, it strongly absorbs the incoming laser radiation and hence, shields the substrate. With increasing laser pulse intensity the plasma plume expands in volume and its forward direction becomes more dominant. With further increase, the plasma decouples from the substrate and propagates in direction towards the incident laser beam. This is often termed as laser supported absorption wave (Bäuerle, 2011). If the propagation velocity is subsonic we denoted it as laser supported combustion wave. In case that the velocity is supersonic, we talk about the laser supported detonation waves.

We can distinguish these main mechanisms of laser induced ns plasma. First, as the laser pulse is impinging to the sample surface, it produces heat on the surface and optical breakdown. Subsequently ionized plasma is formed. Ablated vapour and plasma expands into the ambient atmosphere, producing shock waves, followed by optical emission and particle ejection (Viskup et al., 2009). Later the cooling effect and visible crater produced as a side effect on a surface. Photography of ns laser induced plasma from Nd:YAG laser in air atmosphere is shown in Figure 2.

Fig. 2. Photography of ns laser ablation from Nd:YAG laser in air atmosphere. Ablation of material leads to ejection of cluster particles that may be irradiated by subsequent laser pulses.

2.2 Ionization

Ionization of atoms, molecules and dissociation of molecules within a gas at temperature T occurs at values of $k_B.T$ much lower than the ionization potential. Within a gas, collision between the species – electrons, atoms, molecules results in a certain degree of ionization, ξ. By considering dynamic equilibrium, where the rate of generation is equal to rate of recombination, degree of ionization can be expressed by the Saha equation

$$\frac{\xi^2}{1-\xi} = \frac{2g_i}{g_a N_g}\left(\frac{m_e k_B T}{2\pi\hbar^2}\right)^{\frac{3}{2}} \exp\left(-\frac{E_i}{k_B T}\right) \quad (1)$$

where $N_g = N_i + N_a$ with N_i and N_a the number densities of ions and atoms. The degree of ionization is given by $\xi = N_i / N_g$, and g_i and g_a denote the degeneracy of states for ions and atoms, m_e is the electron mass, k_B is the Boltzmann constant, $\hbar$ is the Planck constant and E_i is the ionization energy. However within the laser matter interaction the Saha equation has only limited validity. Laser light may directly ionize species through sequential or coherent multiphoton excitation or via collisions with electrons accelerated within the laser field – called impact ionization. The diffusion processes of electrons out of the plasma plume and strong non-equilibrium condition have to be also considered.

2.3 Optical breakdown

In principle a fast electron results in two slow electrons, which are again accelerated by the laser radiation, and this cycle is repeating again. In the initial stage of optical breakdown, the concentration of electrons increases exponentially. These processes increase with the number of energetic electrons, which can again ionize atoms or molecules. This avalanche like ionization of the plasma due to laser irradiation is called optical breakdown. In order to estimate the threshold laser intensity for optical breakdown it is necessarily to consider the electron energy losses due to collisions with atoms and electrons. It has been proved that laser-induced breakdown occurs in the range of 10^9 -10^{13} W.cm^{-2}, in air gas at atmospheric pressure and with ns laser pulses (Capitelli, 2004). These values are about three orders of magnitude higher than the values observed in front of solid or liquid targets. This is because the ionized hot material vapours which are present on a target surface. With increasing temperature near the target, the light intensity change due to reflections and the electric field at the fringe of the target surface is enhanced. With high pressures, the electron energy losses are mainly due to collisions with atoms. An estimation of intensity for optical breakdown in ambient gas I_p^{opt} can be made by using following equation:

$$I_p^{opt} \approx \frac{m_e^2 c \omega_c^2 E_i}{2\pi m_g e^2} \propto p^2 \quad (2)$$

where m_e is the electron mass, m_g is the mass of the gas particles, p is the gas pressure and ω_c is the collision frequency.

2.4 Plasma plume expansion

Plasma expansion into vacuum

In a vacuum the plasma plume undergoes free expansion and reaches some final constant velocity. This process can be thought in good approximation to be adiabatic. The fastest expansion occurs along the shortest axis of the plume where the highest pressure gradients are.

Plasma expansion into an ambient atmosphere

The expansion dynamics of the plasma plume change significantly, under ambient gas. This occurs generally since gas pressure exceeds 0.1mbar. The ejected species from the sample substrate behave like a piston. They compress and heat the ambient gas medium. This phenomenon causes an external shock wave pressure, which push the ambient gas away from the contact surface. This situation is schematically shown in Figure 3.

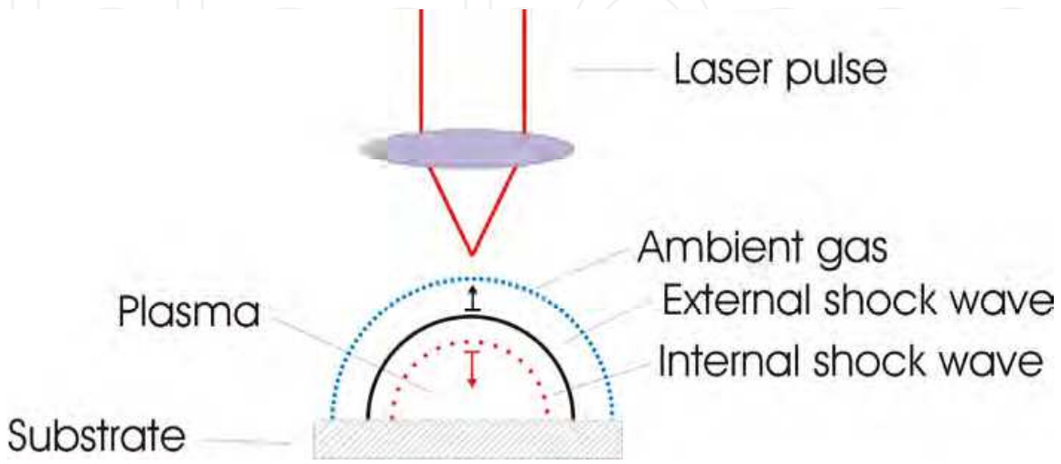

Fig. 3. Schematics showing the expansion of a spherical plasma plume in an ambient medium.

2.5 Expansion models

We can consider different models for the plasma plume expansions dynamics. In analytical model of plasma expansion is assumed that the equations of the gas dynamics can be applied. In this model the Knudsen-layer is not involved and a mixing of the plume and the ambient gas is not considered. The condensation, recombination and excitation are not included. The plasma expansion is of spherical symmetry. Input parameters are initial energy and mass of the plume. Losses due to sample heating, evaporation and plasma shielding are infinitesimal. The overall kinetic energy is conserved in the initial free and adiabatic expansion. The velocity of free expansion scales as

$$v_f \approx \left(\frac{E}{M}\right)^{1/2} \tag{3}$$

where E is the initial energy and M is the mass. This velocity of free expansion is in the range of $10^6 - 10^7 cm.s^{-1}$. Because the plume acts like a piston, an internal shockwave is formed at the contact surface and moves in opposite direction than the plume. Later it propagates in outward direction. This oscillation of the internal shock wave front homogenizes an entire plasma plume. After the plume slow down, its energy becomes mostly thermal and obeys the point blast wave expansion. This occurs when the rest mass in the external shock wave becomes comparable to the mass within the plume.

The radius of the shock wave expansion at medium pressures is given by (Arnold, 1999):

$$R_{SW} = \xi_0 \left(\frac{E_0}{\rho_0} \right)^{\frac{1}{5}} t^{\frac{2}{5}} \tag{4}$$

where ξ_0 is a constant dependent on specific heat capacity. This model describes the explosive energy release E_0 through a background gas density ρ, while it neglects viscosity and predict complete propagation. For calculation of plasma plume expansion radius is also often used the Drag model,

$$R_{DF} = R_0 \left(1 - \exp(-\beta t)\right) \tag{5}$$

where R_0 is the stopping distance of the plasma plume and β is slowing coefficient $\left(R_0 \beta = v_0\right)$ which depend on velocity v_0 of ablated species. This model in the contrast with the previous, predicts that plasma will eventually come to rest due to resistance from collisions with the background gas.

2.6 Validation of the model

To experimentally validate this model an iron oxide sample has been irradiate by Nd:YAG laser at fundamental wavelength λ = 1064 nm, with energy E_L = 100 mJ in air ambient gas. The variation of plasma emission intensity perpendicular to the target surface measured at different delay times are shown in Figure 4(a). The intensity profiles were taken in the plume centre and the intensities were normalized to the highest intensity measured for each delay time. The profiles showed a maximum intensity I_{max} followed by a strong intensity gradient which marked the front of the bright plume. The position for maximum intensity and the plume front shifted to larger distances at longer delay times. An effective plume length R was derived from plume images taken at different time t employing an intensity

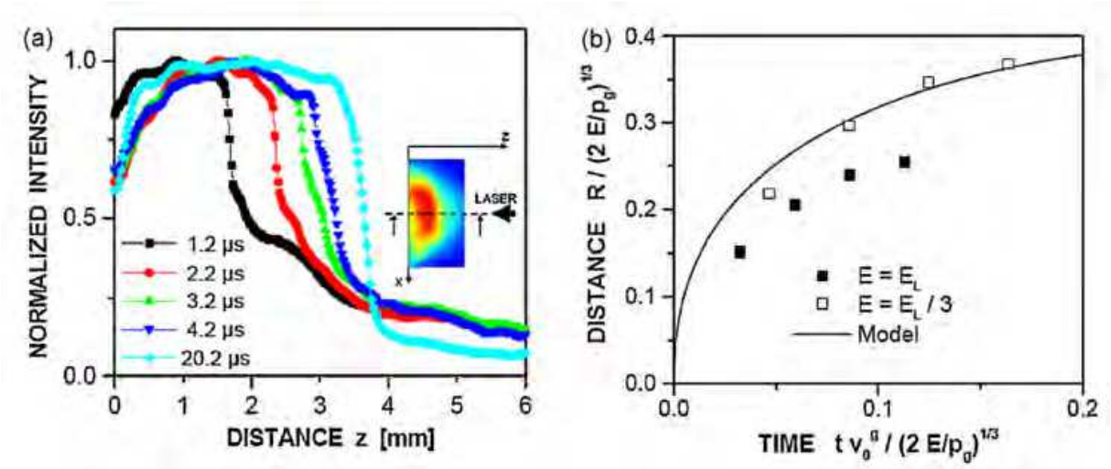

Fig. 4. Intensity profile of plasma emission of iron oxide sample after laser ablation (λ = 1064 nm, E_L = 100 mJ) in air, Fig. 4(a). The dashed line indicates the position of line cut through intensity maps (inset). Comparison of the temporal evolution of iron oxide plasma plume length with model curve shown in Fig. 4(b). Solid and open symbols are obtained assuming an initial plume energy of $E = E_L$ and $E = E_L/3$, respectively (Viskup et al., 2010).

criterion $I = 0.5I_{max}$. The variation of plume length with time is shown in Figure 4(b) in normalized coordinates, with the initial plume energy E, the gas background pressure $p_g = 96.900 Pa$, and the sound velocity in air $v_0^g = 343\,\mathrm{m/s}$. The solid symbols were calculated from the measured plume length assuming an initial plume energy that was equal to the laser pulse energy ($E = E_L = 100$ mJ). The open symbols were calculated for a lower plume energy ($E = E_L/3$) assuming that processes such as melting, vaporization and ejection of materials consumed a large part of the laser pulse energy. The solid line is calculated by a model describing spherical plume expansion into ambient gas. For solid bulk materials such as stainless steel, metal oxides and polymers a good agreement was found between the plume length measured at low background pressure and the model (Huber et al., 2000). At higher pressure additional effects such as hydrodynamic instabilities at the expansion front become relevant (Heitz et al., 2003).

2.7 Ablation mechanisms

Pulsed laser ablation by nanosecond laser pulses has been analyzed on the basis of various models. Depending on initial activation we recognize phototermal ablation, photochemical ablation or combination of both processes - photophysical ablation. These models usually include only single dominant mechanism, therefore they permits to analyze experimental results only partially, depending on material in narrow range of parameters.

The processes involved in phototermal ablation are initiated with single or multi-photon excitation of the irradiated material surface. If the excitation energy is rapidly transformed into heat, it causes the temperature increase at the surface. This affects the overall optical properties of the irradiated material surface and consequence the absorbed laser power. The temperature rise can result in thermal material ablation or vaporization with or without the surface melting. Another possible way is that temperature rise induces stress which can produce explosive type of ablation. The stresses can also change the optical properties and thereby influence the temperature rise.

For photochemical ablation, when the photon energy is sufficiently high, laser excitation can lead to direct bond breaking. Accordingly from the irradiated surface the atoms, molecules clusters or fragments of materials are desorbed into ambient atmosphere. The indirect way to ablation through light induced defects which can photochemically dissociated bonds; this can build up a stress resulting in mechanical ablation. Both these ways can apply in principle without any change at temperature in surface.

In case of photophysical ablation, process both thermal and non-thermal mechanisms contribute to ablation rate. It can be a system in which the lifetime of electronically excited species or broken bonds is sufficiently long. During this time the species can desorbs by the temperature rise from the surface, well before the total excitation energy is entirely dissipated into a heat. The overall processes of photophysical ablation are influenced by thermal or non-thermal defects, stress and volume changes.

Mention possible mechanisms are not complete, due to additional development of plasma emission, mainly the electrons and ions. These can cause additional electric fields, which may change the activation energy for thermal desorption or direct bond breaking.

3. Single laser pulse irradiation

3.1 Basic parameters

Laser induced plasma is a pulsed source, and therefore the optical spectrum evolves rapidly in time. The emission from laser induced plasma generated by single nanosecond laser pulse in air atmosphere is characterized by different processes. An important time periods after laser plasma formation during which emissions from different species predominate are: strong continuum emission, formation of ionized species, emission of neutrals and finally emission of molecules. Depending on measurement is possible to carried out time-resolved detection of optical plasma emission. Corresponding spectra can be monitored by using a gateable detector. To enhanced laser ablation processes, commonly measurements are conducted by using repetitive single pulse irradiation, which mean a series of individual laser pulses, which are formed on the surface of the investigated sample, with laser pulse repetition rate a few hertz.

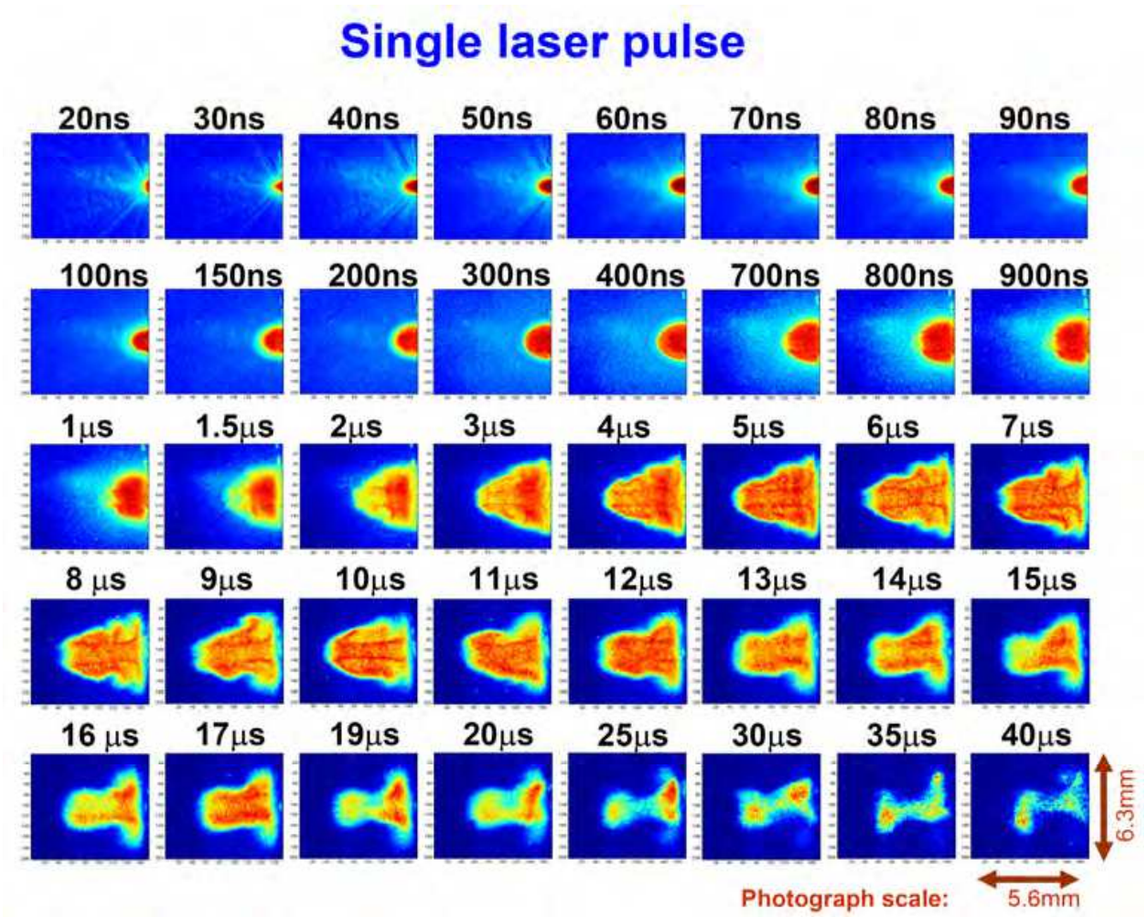

Fig. 5. Time resolved photography of plasma plume expansion from PA (Ultramid®, black) into the air ambient atmosphere. Laser pulse energy E ≈170 mJ, λ_L=532nm, integration time 10ns, photograph scale 5.6mm × 6.3mm. The images are shown in false colour technique encoding the emission intensity normalized to the maximum intensity (dark red) of each image.

3.2 Time resolved plasma photography of single pulse interaction

Time resolved photography of plasma plume expansion from PA (Ultramid®, black) into the air ambient atmosphere is shown in Figure 5. The images are taken at different delay times after the laser pulse ranging from $\Delta\tau_D$=20ns to $\Delta\tau_D$=40μs as indicated above the images. The integration time of the ICCD was set to 10ns. Each image was made with a separate laser pulse. The scale bar 5.6mm × 6.3mm is the same for all images. The images are shown in false colour technique encoding the emission intensity normalized to the maximum intensity (dark red) of each image.

Time resolved photography shows relatively homogeneous evolving plasma plume with approximately hemispherical shape and clearly defined rim, given by the shock front for delay times up to about 1μs after the laser pulse. After this time delay, the rim of the plasma becomes irregular and the plasma starts to detach from the sample surface forming a "mushroom cloud", which is mostly pronounced for a delay time of $\Delta\tau_D$=10μs after the laser pulse. For even later delays, the plasma develops into a perturbed and heterogeneous plume, which is not detectable for the camera any more after about $\Delta\tau_D$=40 μs. An estimation of the absolute intensities of the images is possible with help of the data in Figure 6, which were extracted from the same time resolved photography images. In this figure, the temporal development of not spectrally resolved intensities of the laser-induced plasmas is shown for single-pulse excitation with different time delay. The mean intensities of the recorded images were measured with the fast time-resolved ICCD camera. The spectral range was limited to wavelengths above about 350 nm, which is given by the cut-off of the glass camera objective employed. From this graph we can see that, the plasma intensities decay fast in the first $\Delta\tau_D$=1μs or $\Delta\tau_D$=2μs and then is stabilize on a lower level for considerably longer times, which is only slightly decaying. This is in consistent with the time-resolved plasma plume images, shown in Figure 5.

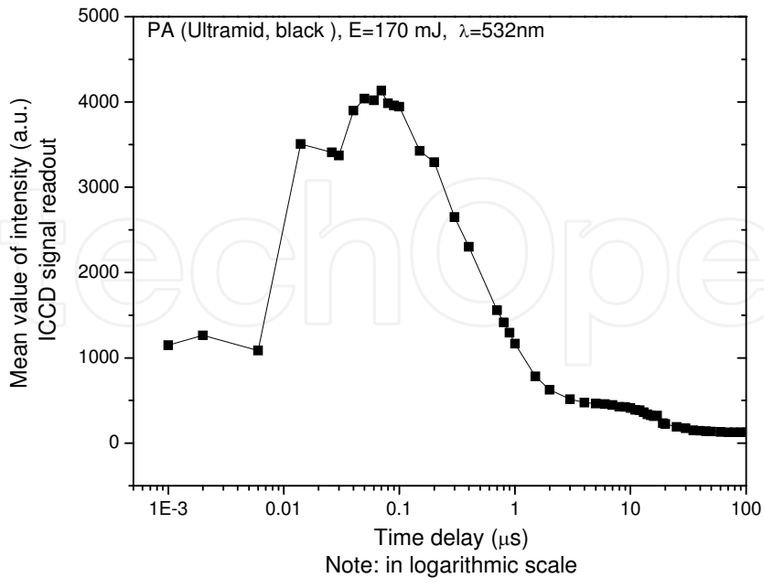

Fig. 6. The mean intensity value derived from time resolved ICCD photography of plasma (PA Ultramid®, black) plume expansion for single laser pulse. The integration time of the ICCD is set to 10 ns for this evaluation.

4. Double or multiple laser pulse irradiation

4.1 Methods of double pulse irradiation

In laser induced plasma spectroscopy technique, very important factors are precision and sensitivity of obtained spectra. Recently, new studies have lead to investigations of multiple-pulse irradiation which can greatly enhanced plasma emission. It has been found that dual-pulse irradiation technique can significantly give enhancement to plasma emission and hence improve the emission from the weak elements. The main idea of double pulse method is based on the formation of pre-ablation plasma on the surface of the studied material, while the second pulse, which is incoming several nanoseconds or microseconds behind the first laser pulse is further enhancing the plasma emission. The important parameter for double pulse laser interaction is the temporal difference between the arrival of the second laser pulses at the target Δt_L , also called interpulse delay or pulse to pulse separation time.

There are two main methods in double pulse irradiation. In first method the first laser pulse generates laser induced plasma at the sample surface, and second laser pulse re-heats a plasma (increased plasma volume, temperature, ion density, expansion and ablation rates, longer decay times) or re-excite material ablated by first laser pulse. In the second method 1st laser pulse generates low pressure region above the sample surface and 2nd pulse generates plasma that expands into low pressure region. This can be generally realised by four commonly used beam geometries for double pulse irradiation measurements, which are schematically shown in Figure 7.

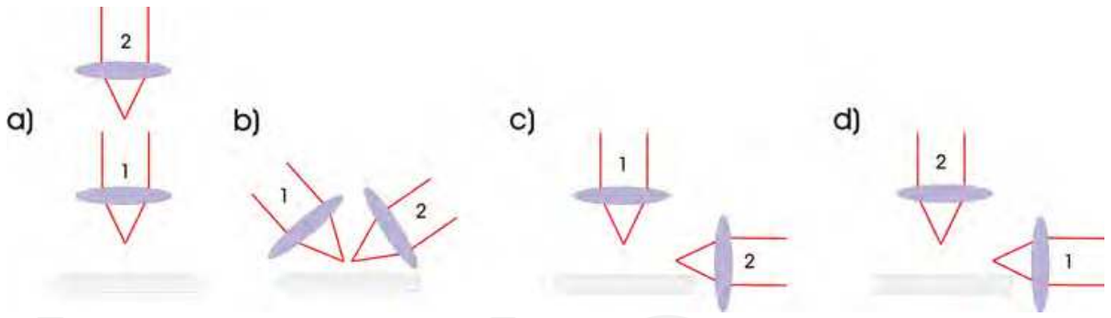

Fig. 7. Commonly used beam geometries for double pulse excitation: a) collinear dual pulse b) crossed beam dual pulse c) orthogonal reheating d) orthogonal pre-ablation dual pulse.

- Collinear dual pulse arrangement, where both pulses are focused upon the same point on the sample.
- Crossed beam dual pulse configuration, where separate two laser pulses under different angles are focused into the same point on the sample surface.
- Orthogonal pre-ablation spark dual pulse configuration in which air plasma is formed above the sample surface prior to ablation.
- Orthogonal reheating configuration, where an air plasma is formed after ablation

4.2 Time resolved plasma plume photography of double pulse interaction

Time-resolved photographic images of collinear double-pulse (DP) plasma plume expansion dynamics from polyamide (Ultramid®, black) into air ambient atmosphere are shown in

Figure 8. Delay between two laser pulses is Δt_L = 20ns. The images are taken at different delay times after the first laser pulse, up to $\Delta\tau_D = 90\mu s$ as indicated above the images. The integration time of the ICCD was set to 10ns. Pictures starts from single laser pulse exposure ($\Delta\tau_D = 10ns$ after the first pulse) and in $\Delta\tau_D = 20$ ns after the first pulse, the second laser pulse is entering. At this time delay, all the energy from first laser pulse is already deposited in polyamide target and plume is expanding. From time resolved photography pictures we can assume, that energy transfer between both laser pulses performed very smoothly, without subsequent disturbances of plasma plume. Plasma plume continuously absorbs energy and continues to growth forming relatively homogeneous evolving plasma plume with approximately hemispherical shape profile up to $\Delta\tau_D = 4\mu s$, similar, as it was in the case of single laser pulse exposure (Figure 5). Later in $\Delta\tau_D = 7\mu s$ the "mushroom" like structure phase of expanding plasma plume is in not so clear and evident as it was in the single pulse mode. For delays of $\Delta\tau_D = 10\mu s$ and longer, the perturbations occur resulting in

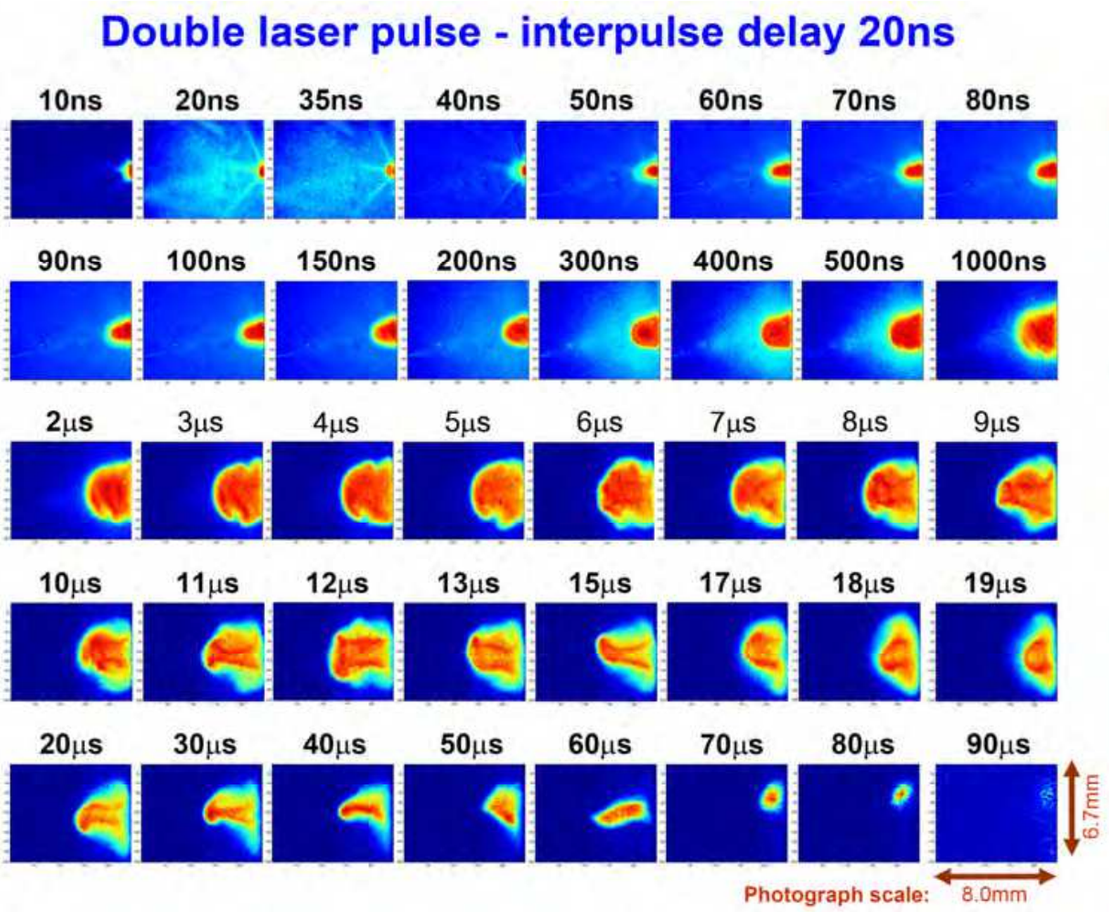

Fig. 8. Time-resolved photographic images of double-pulse (DP) plasma plume expansion from polyamide (PA - Ultramid®, black) into air ambient atmosphere. Delay between two laser pulses is 20 ns, laser pulse energies of $E_1 \approx E_2 \approx 170$ mJ, λ_L=532nm, integration time 10ns, photograph scale 8.0mm × 6.7mm. Pictures start from single pulse exposure ($\Delta\tau_D = 10ns$) and in $\Delta\tau_D = 20$ ns the second laser pulse is entering.

a heterogeneous plasma plume, which finally declines after about $\Delta\tau_D = 90\mu s$. Generally, the time of the different expansion phases of the plasma plume for double pulse excitation are longer than in the single-pulse case.

The first three images in Figure 9 show single-pulse plasma expansion. Then at a delay time of 1 μs after the first laser pulse, the sample is irradiated with the second laser pulse forming a new plasma channel in the single-pulse plasma. Pictures reveals plasma plume conjunction ($\Delta\tau_D$ = 1030ns ÷1060ns), after impact of the second laser pulse to already formed plasma, generated by first laser pulse. The plasma channel expands first vertically to the sample surface ($\Delta\tau_D = 1050$ ns) and then expands mainly in the transverse direction ($\Delta\tau_D = 1100$ ns to $\Delta\tau_D = 5\mu s$) resulting in an appearance homogeneous disk-shaped plasma

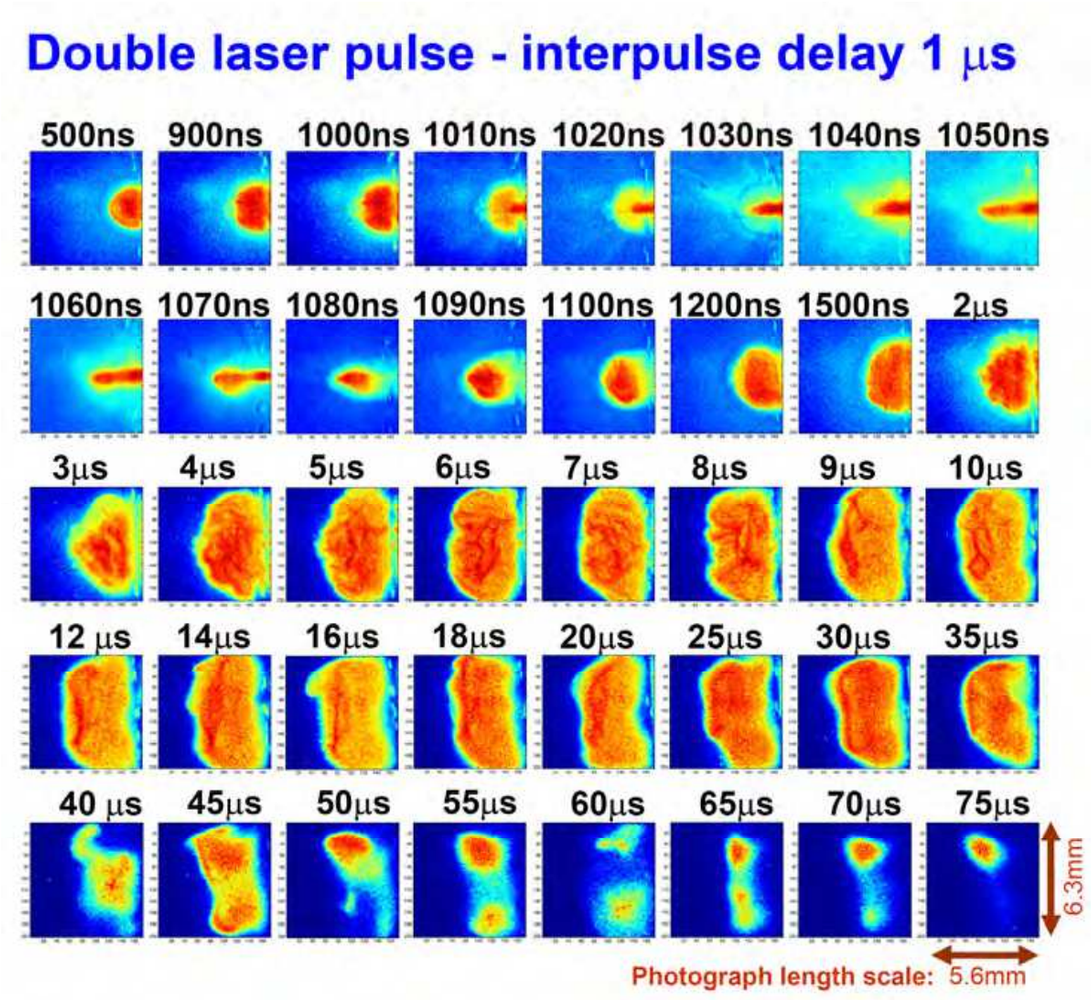

Fig. 9. Time-resolved photographic images of double-pulse (DP) plasma plume expansion from PA (Ultramid®, black) into air ambient atmosphere. Delay between two laser pulses is 1μs, laser pulse energies of $E_1 \approx E_2 \approx 170$ mJ, λ_L=532nm, integration time 10ns, photograph scale 5.6mm × 6.3mm. Pictures start from single laser pulse exposure (500ns, 900ns), followed by second laser pulse in $\Delta\tau_D = 1\mu s$.

with a height of about 3 mm and a diameter of about 7 mm. The size of the plasma remains relatively stable up to a delay time $\Delta\tau_D = 30$ μs. Afterward, it starts to decay from around $\Delta\tau_D = 40$ μs up to approximately $\Delta\tau_D = 80$ μs.

Comparing plasma plume length from Figure 8 and Figure 9 in vertical direction, both cases, plume's length are approximately identical. Whereas in transverse direction, the plume size aggrandise more than double, in the case of DP with Δt_L=1 μs interpulse delay.

Figure 10 shows the plasma expansion images for double-pulse excitation with interpulse delay Δt_L = 10 μs. The first image at a delay time $\Delta\tau_D = 9.999$ ns is the single-pulse plasma of the first laser pulse, which appears again similar to a "mushroom cloud". The following images show the plasma after double-pulse excitation. The picture ($\Delta\tau_D = 10.010$ns) reveal evolving small second plasma (after irradiation of the target by second laser pulse) in the vicinity of the target, inside the already well formed "mushroom" plume, created by first laser pulse.

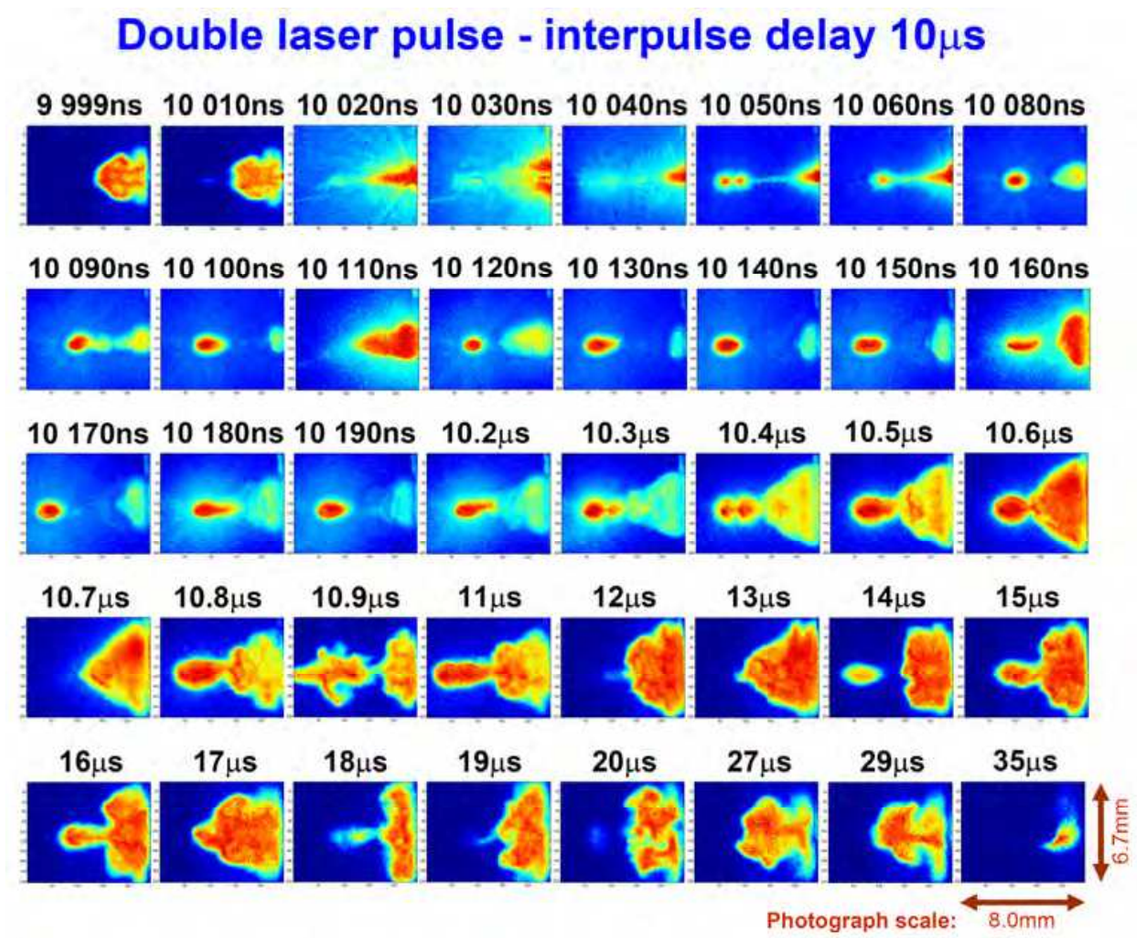

Fig. 10. Time-resolved photographic images of double-pulse (DP) plasma plume expansion from PA (Ultramid®, black) into air ambient atmosphere. Delay between two laser pulses is 10μs, laser pulse energies of $E_1 \approx E_2 \approx 170$ mJ, λ_L=532nm, integration time 10ns, photograph scale 8.0mm × 6.7mm. Pictures start from single laser pulse exposure (9 999ns) and since 10μs the second laser pulse is entering.

Conjunction of plasma plume in $\Delta\tau_D = 10.020$ns takes a place, plasma from second laser pulse further continue to grow. In $\Delta\tau_D = 10.050$ns plume starts to split into islands or droplet, connecting to channels, which last up to approximately $\Delta\tau_D \approx 10.200$ns. During this evolving time delay might happen that these two plasmas are again joining (see $\Delta\tau_D = 10.110$ns) or re-joining. Both plasmas are further expanding in $\Delta\tau_D = 10.400$ns. In later time delay $\Delta\tau_D = 18$µs plume starts to decay but persist up to $\Delta\tau_D = 40$µs.

We can outline, that for Δt_L =10µs pulse separation we obtained unstable heterogonous plasma expansion behaviour. This distortion in plasma plume (islands or droplet) can be also due to the interaction of the incoming second laser beam with ejected solid or liquid particles resulting from the first irradiation. Therefore plasma generated by second laser pulse divers and created structure can appear with randomized re-joining shape. Because each image is made with a separate laser pulse, the evaluation of the dynamic behaviour based on similarities of consecutive images is not clearly visible. Plume does not last longer in this case, and is approximately comparable with duration of single pulse irradiation.

The temporal development of not spectrally resolved intensities of the laser-induced plasmas is shown in Figure 11 for single-pulse and double-pulse excitation with different interpulse-delay times, Δt_L. The mean intensities of the recorded images were measured with the fast time-resolved ICCD camera.

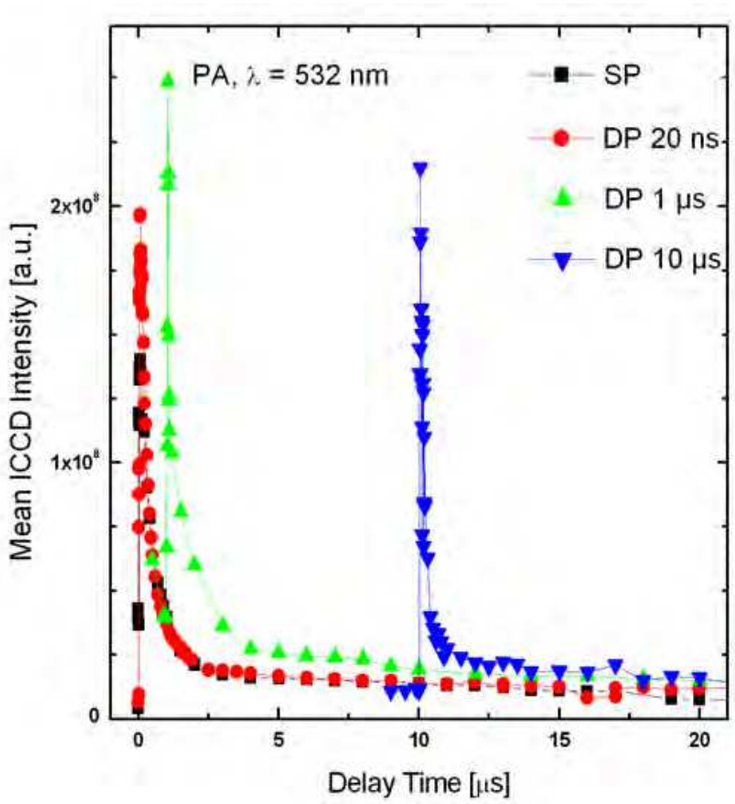

Fig. 11. Single-pulse (SP) and double-pulse (DP) mean intensity derived from time resolved ICCD photography of plasma plume expansion. The integration time of the ICCD is set to 10 ns. Interpulse delay is Δt_L= 20 ns, Δt_L= 1 µs, and Δt_L= 10 µs.

For the double-pulse excitations with Δt_L = 1μs and Δt_L=10μs, only the decay after the second pulse and the time shortly before the second pulse are shown. The images for single-pulse and double-pulse excitation with Δt_L = 1μs and for double-pulse excitation with Δt_L = 20 ns and Δt_L=10μs were recorded in two independent experiments with slightly different gain and magnification. This was corrected by multiplication of a factor in order to obtain consistent overlaps of the different curves. In all four cases, the plasma intensities decay fast in the first 1μs or 2μs and then stabilize on a lower level for considerably longer times, which is only slightly decaying. The intensity of the double-pulse plasma with Δt_L = 1μs starting in the shoulder of the single-pulse excitation is considerably more intense than the single-pulse plasma and also the double-pulse plasmas with Δt_L = 20 ns and Δt_L=10μs.

5. Emission processes in plasma

5.1 Basic mechanisms

In plasma atoms and ions particles undergo transitions between their quantum states through collisional and radiative processes. Among these processes the most important are spontaneous radiative transitions and collisional transitions induced by electron impact collisions.

After absorption of the intense short laser beam, the plasma has sufficient energy to emit radiation via free-free, free-bound and bound-bound mechanisms. Free-free or Bremsstrahlung emission occurs when a free electron interacts with the Coulomb potential of the ions, and radiates a continuum electromagnetic spectrum. The second process also produces a continuum electromagnetic spectrum due to electron transitions from initial free electron states to bound electron states. This mechanism is known as recombination radiation. The last emission mechanism produces a line spectrum as a result of transitions between discrete bound levels of ionized and neutral atoms.

Significant contribution to plasma emission is due to electron-ion recombination processes. The recombination processes gives rise to continuum emission at photon energies greater than the ionization energy of the recombining ion. In plasma where exists simultaneously two or more ionized states, spectral emission is characterized by characteristic jumps, related to different ionization energies, also known as recombination edges.

5.2 Line emissions

Transitions of bound electrons from excited states to lower states of ions and neutrals emit radiation with discrete energy. This could take place in the ground state where strong emission is produced or between excited states where relatively weak radiation is emitted. The emitted intensity of an atomic, ionic, or molecular spectral line is proportional to the population of the upper level, to the transition probability, and to the energy of the quantum. Due to different processes in the plasma, the line shows a spectral profile instead of sharp wavelength emitted over a spectral range. According to Boltzmann statistics the proportionality of the optical emission line intensity I_λ^{ij} corresponding to the transition at certain wavelength between two energy levels E_u and E_l of an atom or ion is given by the formula

$$I_{\lambda}^{ul} = F.A_{ul}.h.\nu_{ul}\frac{n_i}{Z_i}g_{i,u}\exp\left(-\frac{E_{iu}}{kT_{ex}}\right) \quad (6)$$

where

F is the factor depending upon experimental setup;
A_{ul} is the corresponding transition probability per unit time
h is the Planck's constant;
ν_{ul} is the frequency of the photons emitted due to transition from upper excited level u to the lower level l;
n_i is the concentration of the chemical species i;
Z_i is the partition function of the chemical species i calculated at T_{ex}
$g_{i,u}$ is the statistical weight of the upper excited state of the chemical species i;
E_{iu} is the energy of the upper excited state of chemical species i;

It the case of using this equation it is necessary to assume that plasma is homogeneous, is in local thermal equilibrium and also that plasma is optically thin, which mean that emitted photons are not re-absorbed.

The power radiated per unit volume, solid angle and frequency interval, corresponding to the transition from the upper state to the lower state. Level populations and shape of line emission depend on the physical conditions in the plasma and are determined by the dynamical balance of several collisional and radiative processes inside the plasma. Three physical processes which influence the shape of line emission are: a) natural broadening due to the finite lifetime of the states involved in the transition, b) Doppler broadening due to thermal motion, c) pressure broadening due to the interaction of the radiating systems with the rest of the plasma and d) Stark broadening due to charged perturbers.

5.3 The effect of double pulse laser interaction to plasma emission

Figure 12 shows single-pulse versus double-pulse plasma optical spectra of polyamide with interpulse-delay times, Δt_L, of 20 ns, 1 μs, and 10 μs. In spectra are dominating emission from atomic and ionic C, N, H, O, Ca, or Mg lines originating from the PA, additives in the PA, or the surrounding air atmosphere. Strong lines are visible from carbon main matrix compound (C I at 247.86 nm), trace element calcium (Ca II at 393.37nm), and H(α) Balmer series line at 656.3nm. The lines are seated on a pronounced continuum with a periodical structure, especially for the single-pulse spectrum and the double-pulse spectrum with Δt_L = 20 ns. The periodical structure of the continuum results are from the different diffraction orders of the Echelle spectrometer, which has for each diffraction order a lower sensitivity at the rim compared to the centre of the order. Additionally, molecular emission of moderate and weak intensity is visible, e.g., the CN violet band with band-head at 388 nm and the C_2 Swan band with band-head at 516nm. With longer interpulse-delay times the continuum gets weaker and some atomic lines get sharper. This is especially visible for the width of the H(α) line. However, most of the other atomic lines are pronounced for the double-pulse spectrum with Δt_L = 1 μs. They are considerably weaker for the single-pulse spectrum, which has only half of the total laser energy, but also for the double-pulse spectra with Δt_L = 20 ns and Δt_L=10 μs.

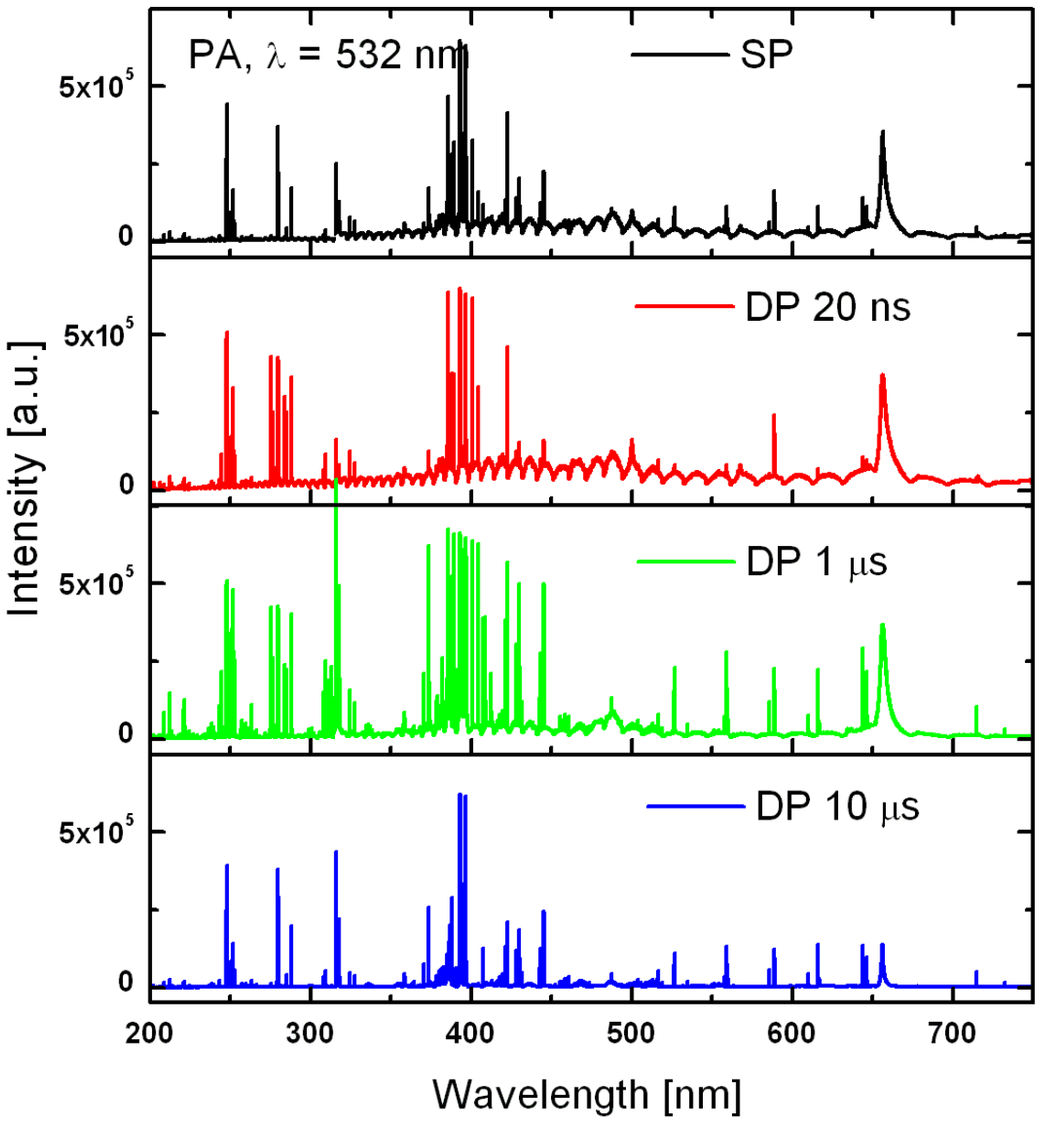

Fig. 12. Single-pulse and double-pulse optical spectra of polyamide plasma. ($E_1 \approx 170$ mJ or $E_1 \approx E_2 \approx 170$ mJ, λ_L=532nm, $\Delta\tau_G$=25μs, $\Delta\tau_D$=500ns). Delay times between the pulses: Δt_L of 20 ns, 1 μs, and 10 μs. All spectra are accumulated over 20 laser pulses.

6. Conclusions

This chapter has presented experimental results on single and double ns laser pulse interaction with solid state with application to plasma spectroscopy. We have applied a collinear nanosecond double pulse exposure of target materials to enhance an optical emission from plasma. Beside of these studies, a plasma from single and double pulse irradiation has been analysed by means of time resolved plasma plume photography and spectroscopy. We compare these results and we find out a very good relation between shape of plasma plume and plasma emission.

From single laser pulse interaction the time–resolved photography shows a relatively homogeneous evolving plasma plume with approximately hemispherical shape and clearly defined rim, given by the shock front for delay times up to ~1μs after the laser pulse. For later time delay, the rim of the plasma plume becomes irregular and the plasma starts to detach from the sample surface forming a "mushroom cloud", which is most pronounced for a delay time about ~10μs after the laser pulse. For even later delays, the plasma develops into a perturbed and heterogeneous plume, which is not detectable for the camera any more after ~40μs. The main atomic and ionic emission signal in studied plasma last approximately ~7μs, while the molecular emission from plasma last approximately ~50μs in air atmosphere.

To enhance a plasma emission from single pulse, we performed collinear nanosecond double-pulse excitation. Special attention has been given to interpulse-delay between 20ns to 10 μs. The similar measurement of time resolved plasma plume photography and time resolved spectroscopy were performed. It has been find out that after double pulse laser impact with short interpulse delay (20ns), plasma seems to expand also relatively homogenously and last significantly longer, compared with to only single pulse exposure. In a case of very long interpulse delay approximately 10μs, formed plasma plume is very heterogonous and plasma emission last similar time as single pulse plasma.

Double-pulse excitation can result in enhanced emission of atomic and ionic spectral lines. We observed a strong influence of pulse-to-pulse delay on the results of 532 nm double-pulse irradiation. We attribute this interdependence to the different plasma expansion dynamics observed by time-resolved photography with different pulse-to-pulse delays. A further enhancement in signal intensity and sensitivity seems to be feasible by optimization of the timing of the interpulse-delay times between the laser pulses. However, the optimal time parameters depend on the specific type of the irradiated material and the individual elemental spectral line under investigation.

7. Acknowledgment

This work has been supported by the Christian Doppler Research Association (Austria). Author would like to thank Prof. Johannes David Pedarnig and Prof. Johannes Heitz for valuable discussions.

8. References

Anisimov S. I., Bäuerle D. & Luk'yanchuk B. S. (1993). Gas dynamics and film profiles in pulsed-laser deposition of materials, *Physical Review B*, Vol.48, pp. 12076–12081.

Arnold N. (1999). Spherical expansion of the vapor plume into ambient gas: an analytical model, *Applied Physics A*, Vol.69, pp. 87.

Babushok V.I., DeLucia F.C., Gottfried J.L., Munson C.A. & Miziolek A.W. (2006). Double pulse laser ablation and plasma: laser induced breakdown spectroscopy

signal enhancement, *Spectrochimica Acta Part B: Atomic Spectroscopy*, Vol.61, pp. 999–1014.

Bäuerle D. (2011). *Laser Processing and Chemistry* (4thed ed.), Springer, ISBN 978-3642176128, Berlin.

Capitelli M. (2004). Laser induced plasma expansion: theoretical and experimental aspects, *Spectrochimica Acta Part B: Atomic Spectroscopy*, Vol.59, pp. 271.

Cremers D.A., Radziemski L.J. & Loree T.R. (1984). Spectrochemical analysis of liquids using the laser spark, *Applied Spectroscopy*,Vol.38, pp. 721–729.

Cristoforetti G., Legnaioli S., Pardini L., Palleschi V., Salvetti A. & Tognoni E. (2006). Spectroscopic and shadowgraphic analysis of laser induced plasmas in the orthogonal double pulse pre-ablation configuration, *Spectrochimica Acta Part B: Atomic Spectroscopy*, Vol.61, pp. 340–350.

Gautier C., Fichet P., Menut D., Lacour J.L., Hermite D. L. & Dubessy J. (2005). Main parameters influencing the double-pulse laser-induced breakdown spectroscopy in the collinear beam geometry, *Spectrochimica Acta Part B: Atomic Spectroscopy*, Vol.60, pp. 792–804.

Heitz J., Gruber J., Arnold N., Bäuerle D., Ramaseder N., Meyer W. & Hochörtler J. (2003). In situ analysis of steel under reduced ambient pressure by laser-induced breakdown spectroscopy, *Proceedings of SPIE, XIV International Symposium on Gas Flow, Chemical Lasers, and High-Power Lasers*, Vol.5120, pp. 588, ISBN: 9780819449801.

Huber N., Gruber J., Arnold N., Heitz J. & Bäuerle D. (2000). Time-resolved photography of the plasma-plume and ejected particles in laser ablation of polytetrafluoroethylene, *Europhysics Letters,* Vol. 51, pp. 674.

Choi S., Oh M., Lee Y., Nam S., Ko D. & Lee J. (2009). Dynamic effects of a pre-ablation spark in the orthogonal dual-pulse laser induced breakdown spectroscopy, *Spectrochimica Acta Part B: Atomic Spectroscopy*, Vol.64, pp. 427–435.

Noll R., Sattmann R., Sturm V. & Winkelmarm S. (2004). Space and time-resolved dynamics of plasmas generated by laser double pulses interacting with metallic samples, *Journal* of Analytical Atomic *Spectrometry,* Vol.19, pp. 419–428.

Peter L. & Noll R. (2007). Material ablation and plasma state for single and collinear double pulses interacting with iron samples at ambient gas pressures below 1 bar, *Applied Physics B*, Vol.86, pp. 159–167.

Sattmann R., Sturm V. & Noll R. (1995). Laser-induced breakdown spectroscopy of steel samples using multiple Q-switch Nd:YAG laser pulses, *Journal of Physics D: Applied Physics*, Vol.28, pp. 2181–2187.

Semerok A. & Dutouquet C. (2004). Ultrashort double pulse laser ablation of metals, *Thin Solid Films*, Vol.453, pp. 501–505.

Viskup R., Praher B., Stehrer T., Jasik J., Wolfmeir H., Arenholz E., Pedarnig J. & Heitz J. (2009). Plasma plume photography and spectroscopy of Fe - oxide materials, *Applied Surface Science*, Vol.255, No.10, pp. 5215-5219.

Viskup R. (2010). Laser Assisted Diagnostics of Industrial Materials, PhD. Dissertation, Johannes Kepler University Linz, Austria.

Viskup R., Praher B., Linsmeyer T., Scherndl H., Pedarnig J.D. & Heitz J. (2010). Influence of pulse-to-pulse delay for 532 nm double-pulse laser-induced breakdown spectroscopy of technical polymers, *Spectrochimica Acta Part B: Atomic Spectroscopy*, Vol.65, pp. 935.

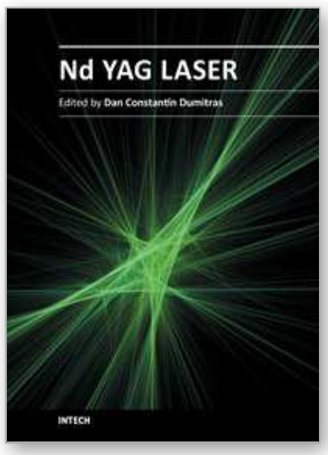

Nd YAG Laser

Edited by Dr. Dan C. Dumitras

ISBN 978-953-51-0105-5
Hard cover, 318 pages
Publisher InTech
Published online 09, March, 2012
Published in print edition March, 2012

Discovered almost fifty years ago at Bell Labs (1964), the Nd:YAG laser has undergone an enormous evolution in the years, being now widely used in both basic research and technological applications. Nd:YAG Laser covers a wide range of topics, from new systems (diode pumping, short pulse generation) and components (a new semiorganic nonlinear crystal) to applications in material processing (coating, welding, polishing, drilling, processing of metallic thin films), medicine (treatment, drug administration) and other various fields (semiconductor nanotechnology, plasma spectroscopy, laser induced breakdown spectroscopy).

How to reference

In order to correctly reference this scholarly work, feel free to copy and paste the following:

Richard Viskup (2012). Single and Double Laser Pulse Interaction with Solid State – Application to Plasma Spectroscopy, Nd YAG Laser, Dr. Dan C. Dumitras (Ed.), ISBN: 978-953-51-0105-5, InTech, Available from: http://www.intechopen.com/books/nd-yag-laser/single-and-double-laser-pulse-interaction-with-solid-state-application-to-plasma-spectroscopy

INTECH
open science | open minds

InTech Europe
University Campus STeP Ri
Slavka Krautzeka 83/A
51000 Rijeka, Croatia
Phone: +385 (51) 770 447
Fax: +385 (51) 686 166
www.intechopen.com

InTech China
Unit 405, Office Block, Hotel Equatorial Shanghai
No.65, Yan An Road (West), Shanghai, 200040, China
中国上海市延安西路65号上海国际贵都大饭店办公楼405单元
Phone: +86-21-62489820
Fax: +86-21-62489821

IntechOpen